

# Establishment of $M1$ multipolarity of a $6.5 \mu_N^2$ resonance in $^{172}\text{Yb}$ at $E_\gamma = 3.3 \text{ MeV}$

A. Schiller,<sup>1,\*</sup> A. Voinov,<sup>2</sup> E. Algin,<sup>1,3,4,5</sup> J.A. Becker,<sup>1</sup> L.A. Bernstein,<sup>1</sup>  
P.E. Garrett,<sup>1</sup> M. Guttormsen,<sup>6</sup> R.O. Nelson,<sup>7</sup> J. Rekstad,<sup>6</sup> and S. Siem<sup>6</sup>

<sup>1</sup>Lawrence Livermore National Laboratory, L-414, 7000 East Avenue, Livermore, California 94551

<sup>2</sup>Frank Laboratory of Neutron Physics, Joint Institute of Nuclear Research, 141980 Dubna, Moscow region, Russia

<sup>3</sup>North Carolina State University, Raleigh, North Carolina 27695

<sup>4</sup>Triangle Universities Nuclear Laboratory, Durham, North Carolina 27708

<sup>5</sup>Department of Physics, Osmangazi University, Meselik, Eskisehir, 26480 Turkey

<sup>6</sup>Department of Physics, University of Oslo, N-0316 Oslo, Norway

<sup>7</sup>Los Alamos National Laboratory, MS H855, Bikini Atoll Road, Los Alamos, New Mexico 87545

Two-step-cascade spectra in  $^{172}\text{Yb}$  have been measured after thermal neutron capture. They are compared to calculations based on experimental values of the level density and radiative strength function (RSF) obtained from the  $^{173}\text{Yb}(^3\text{He},\alpha\gamma)^{172}\text{Yb}$  reaction. The multipolarity of a  $6.5(15) \mu_N^2$  resonance at  $E_\gamma = 3.3(1) \text{ MeV}$  in the RSF is determined to be  $M1$  by this comparison.

PACS numbers: 25.40.Lw, 25.20.Lj, 24.30.Gd, 27.70.+q

Excited nuclei decay often by a cascade of  $\gamma$  rays. While the decay between discrete states is determined by the details of the nuclear wavefunctions, unresolved transitions are best described by statistical concepts like a continuous radiative strength function (RSF) and level density. The RSF (reviewed in [1]) provides the mean value of the decay probability for a given  $\gamma$ -ray energy  $E_\gamma$ . For hard  $\gamma$  rays, ( $\sim 7$ – $20 \text{ MeV}$ ), the RSF is governed by the giant electric dipole resonance whose parameters are determined from photoabsorption [2]. The soft tail of the RSF has been investigated by a variety of methods, most notably by primary  $\gamma$  rays [3]. Recently, systematic studies of the soft RSF have been performed at the Oslo Cyclotron Laboratory using a method based on sequential extraction. With this method it is possible to obtain the level density and RSF by a deconvolution of a set of primary  $\gamma$  spectra from a range of excitation energies [4]. Total RSFs (summed over all multiplicities) of rare earth nuclei can be extracted for  $B_n > E_\gamma > 1 \text{ MeV}$  [5]. Their common, most striking feature is a resonance at  $E_\gamma \sim 3 \text{ MeV}$  which is believed to be of dipole nature but whose electromagnetic character is unknown. It has been shown for all investigated rare earth nuclei that the total RSF is most readily decomposed into a sum of the Kadenskii-Markushev-Furman (KMF)  $E1$  model [6], a spin-flip  $M1$  model [7], and the aforementioned soft dipole resonance [5]. The knowledge of the character of this resonance is essential for its theoretical interpretation. Experimentally, it can be determined from a two-step-cascade (TSC) measurement [8].

The TSC method is based on the observation of decays from an initial state  $i$  to a final state  $f$  via one, and only one, intermediate level  $m$  [9, 10]. A convenient initial state is that formed in thermal or average resonance capture (ARC); the final state can be any low-lying discrete state. TSC spectra are determined by the branching ratios of the initial and intermediate states (expressed as ratios of partial to total widths  $\Gamma$ ) and by the level den-

sity  $\rho$  of intermediate states with spin and parity  $J_m^\pi$

$$I_{if}(E_1, E_2) = \sum_{XL, XL', J_m^\pi} \frac{\Gamma_{im}^{XL}(E_1)}{\Gamma_i} \rho(E_m, J_m^\pi) \frac{\Gamma_{mf}^{XL'}(E_2)}{\Gamma_m} + \sum_{XL, XL', J_{m'}^\pi} \frac{\Gamma_{im'}^{XL}(E_2)}{\Gamma_i} \rho(E_{m'}, J_{m'}^\pi) \frac{\Gamma_{m'f}^{XL'}(E_1)}{\Gamma_{m'}}. \quad (1)$$

The sums in Eq. (1) are restricted to give valid combinations of the level spins and parities and the transition multiplicities  $XL$ . They arise since one determines neither the ordering of the two  $\gamma$  rays, nor the multiplicities of the transitions nor the spins and parities of the intermediate levels, hence one has to include all possibilities. The two transition energies are correlated by  $E_1 + E_2 = E_i - E_f$ , thus, TSC spectra can be expressed as spectra of one transition energy  $E_\gamma$  only. TSC spectra are symmetric around  $E_\gamma^{\text{sym}} = (E_i - E_f)/2$ ; integration over  $E_\gamma$  yields twice the total TSC intensity  $I_{if}$  if both  $\gamma$  rays are counted in the spectra. The knowledge of the parities  $\pi_i$  [11] and  $\pi_f$  ensures that  $I_{if}$  depends roughly speaking on the product of two RSFs around  $E_\gamma^{\text{sym}}$  [8], i.e.,  $f_{E1}^2 + f_{M1}^2$  for  $\pi_i = \pi_f$  and  $2f_{E1}f_{M1}$  for  $\pi_i \neq \pi_f$ .  $I_{if}$  depends also on the level density. This usually prevents drawing firm conclusions from TSC experiments alone [10]. A combined analysis of Oslo-type *and* TSC experiments, however, enables one to establish the sum *and* product, respectively, of all contributions to  $f_{M1}$  and  $f_{E1}$  at energies of the soft resonance, thus determining its character. For this goal, the partial widths of Eq. (1) are expressed via

$$\Gamma_{x \rightarrow y}^{XL}(E_\gamma) = f_{XL}(E_\gamma) E_\gamma^{2L+1} D_x \quad (2)$$

in terms of RSFs and level spacings  $D_x$ . Eq. (2) actually gives only the average value of the Porter-Thomas distributed partial widths [12]. The total width  $\Gamma$  is the sum of all partial widths. Again, the sum is only the sum

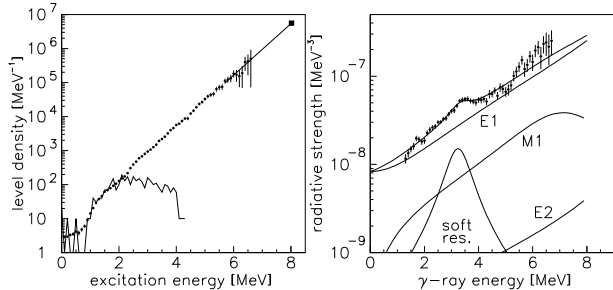


FIG. 1: Left panel: total level density (filled circles), constant-temperature extrapolation (solid line), level density at  $B_n$  from average neutron resonance spacing (filled square) [7], and level density from counting of discrete levels (jagged line) [19]. Right panel: total RSF (filled circles), fit to the data, and decomposition into RSFs of different multiplicities (solid lines). Inclusion of the soft resonance in the fit decreases  $\chi_{\text{red}}^2$  from  $\sim 7.4$  to  $\sim 1.3$ . Since this value is close to unity, inclusion of additional non-statistical structures cannot significantly improve the fit.

of mean values, however, the distribution of total widths with many components is almost  $\delta$ -like [12]. The level density for a given spin and parity is calculated from the total level density by [13]

$$\rho(E_x, J_x^\pi) = \rho(E_x) \frac{1}{2} \frac{2J_x + 1}{2\sigma^2} \exp\left[-\frac{(J_x + 1/2)^2}{2\sigma^2}\right], \quad (3)$$

where  $\sigma$  is the spin cut-off parameter, and we assume equal numbers of positive and negative parity levels. This assumption and Eq. (3) have been verified from the discrete level schemes of rare earth nuclei [14]. Thus, all quantities for calculating TSC spectra are based on experimental data.

The combined analysis is applied to the nucleus  $^{172}\text{Yb}$  which has been investigated by the  $^{173}\text{Yb}(^3\text{He}, \alpha\gamma)^{172}\text{Yb}$  reaction in Oslo and by the  $^{171}\text{Yb}(n, \gamma\gamma)^{172}\text{Yb}$  reaction at the Lujan Center of the Los Alamos Neutron Science Center (LANSCE). The Oslo data have been reported in [4, 5]. Thus, only a short summary is given. The experiment was performed using a 45-MeV  $^3\text{He}$  beam on a metallic, enriched, self-supporting target. Ejectiles were identified and their energies measured using particle telescopes at  $45^\circ$ . In coincidence with  $\alpha$  particles,  $\gamma$  rays were detected in an array of 28 NaI detectors. From the reaction kinematics,  $\alpha$  energy is converted into  $E_x$ , and  $\gamma$  cascade spectra are constructed for a range of  $E_x$  bins. The  $\gamma$  spectra are unfolded [15] and the primary  $\gamma$  spectra are extracted using a subtraction method [16]. The spectra are deconvoluted into a level density and a total RSF by applying the Brink-Axel hypothesis [17]. The level density is normalized by comparison to discrete levels at low  $E_x$  and to the average neutron resonance spacing at  $B_n$  [4]. The RSF is normalized using the average total width of neutron resonances, and is decomposed into the

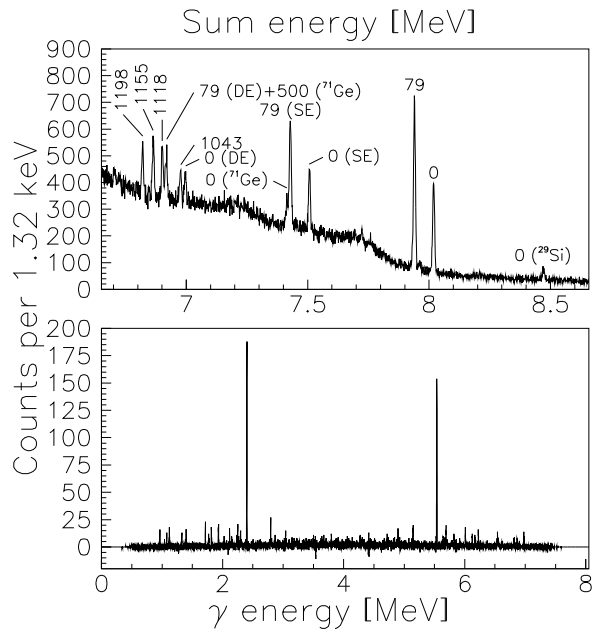


FIG. 2: Upper panel: energy-summed coincidence spectrum from the  $^{171}\text{Yb}(n, \gamma\gamma)^{172}\text{Yb}$  reaction. Peaks are labeled by the energy of the final state. Peaks denoted by  $^{71}\text{Ge}$  and  $^{29}\text{Si}$  are due to  $n$ -capture in the detector and in the glass ampoule, respectively. SE and DE stands for single and double escape peaks, respectively. Lower panel: TSC spectra to the  $2_1^+$  state. The slight asymmetry is due to the energy-dependent resolution of the detectors.

KMF  $E1$  model, a spin-flip  $M1$  model, and a soft dipole resonance [5]. Here, we have improved the normalization of the level density and the RSF and included an isoscalar Lorentzian  $E2$  model [18] giving

$$f_{\text{tot}} = K(f_{E1} + f_{M1}) + E_\gamma^2 f_{E2} + f_{\text{soft}}, \quad (4)$$

where  $K$  is a scaling factor of the order of one. Since quadrupole transitions populate levels within a broader spin interval than dipole transitions, Eq. (4) is of an approximative nature. Given the weakness of quadrupole transitions and the level of experimental uncertainties, however, this approximation is believed to be sufficient. The improved data, the fit to the total RSF, and its decomposition into different multiplicities are given in Fig. 1. The parameters for the  $E1$  RSF are taken from [5], those for the  $M1$  and  $E2$  RSFs from [7], where we use the  $f_{E1}/f_{M1}$  systematics at  $\sim 7$  MeV giving values in agreement with ARC work [20]. The fit parameters are: the constant temperature of the KMF model  $T = 0.34(3)$  MeV, the normalization coefficient  $K = 1.7(1)$ , and the three parameters of the soft resonance  $E = 3.3(1)$  MeV,  $\Gamma = 1.2(3)$  MeV, and  $\sigma = 0.49(5)$  mb [21].

For the  $^{171}\text{Yb}(n, \gamma\gamma)^{172}\text{Yb}$  experiment, we used  $\sim 1$  g of enriched, dry  $\text{Yb}_2\text{O}_3$  powder encapsulated in a glass

ampoule, mounted in an evacuated beam tube and irradiated by collimated neutrons with a time-averaged flux of  $\sim 4 \times 10^4$  neutrons/cm<sup>2</sup>s at  $\sim 20$  m from the thermal moderator.  $\gamma$  rays were detected by two 80% and one shielded and segmented  $\sim 200\%$  clover Ge(HP) detector, placed at  $\sim 12$  cm from the target in a geometry to minimize angular correlation effects and contributions from higher multiplicity cascades. Single and coincident  $\gamma$  rays were recorded simultaneously. The experiment ran for  $\sim 150$  h yielding  $\sim 10^7$  coincidences. The relative detector efficiencies from 1–9 MeV were determined by two separate runs of  $\sim 12$  h each, before and after the  $^{171}\text{Yb}(n, \gamma\gamma)^{172}\text{Yb}$  experiment, using the  $^{35}\text{Cl}(n, \gamma)^{36}\text{Cl}$  reaction and its known  $\gamma$  intensities [22]. Also, a standard calibrated  $^{60}\text{Co}$  source has been measured to adjust the relative curves to an absolute scale. The energy-summed coincidence spectrum (Fig. 2, upper panel) shows distinct peaks corresponding to TSCs between  $B_n$  and several low-lying states. The two strongest peaks have  $\sim 4000$  counts each. TSC spectra (lower panel) were obtained by gating on four peaks. Relative intensities of primary versus secondary  $\gamma$  rays were determined from singles spectra and are in agreement with Ref. [20]. Absolute primary intensities were determined by using new data on absolute secondary  $\gamma$ -ray intensities [23] and subsequent scaling of primary intensities to these values using the relative intensities of [20]. These absolute primary intensities are  $\sim 20\%$  higher than in [20]. TSC intensities are normalized to (i) the absolute primary intensity and secondary branching ratio of one, strong, individual TSC and (ii) by effectively estimating the number of neutron captures during the experiment from secondary singles lines, their absolute intensities, and absolute detector efficiencies. Both methods give equal results within the error bars.

TSC spectra are compared to calculations according to Eq. (1) assuming either electric or magnetic character for the soft resonance [8]. Due to Porter-Thomas fluctuations of TSC intensities, TSC spectra are compressed to  $\sim 300$  keV energy bins and only a  $\sim 2.4$  MeV broad energy interval in the middle of the spectra is taken into account [10] for comparison. Corrections due to non-isotropic angular correlations of TSCs have been estimated to be less than  $\sim 3\%$  and are thus neglected. Contributions to the thermal radiative neutron capture cross section  $\sigma_{n,\gamma}^{\text{th}}$  from the two possible spins ( $0^-$  and  $1^-$ ) involved in neutron  $s$ -capture on  $^{171}\text{Yb}$  are uncertain. The compilation [24] assumes  $0^-$  for the sub-threshold resonances which contribute 88% to  $\sigma_{n,\gamma}^{\text{th}}$ . Another 4% comes from  $0^-$  resonances above threshold, giving in total a 92% contribution of  $0^-$  states. On the other hand, there is no strong evidence that all contributing sub-threshold resonances have  $0^-$ . Examination of hard primary  $\gamma$ -rays [20, 25] reveals many strong transitions populating  $2^+$  levels, indicating that a sizeable portion of  $\sigma_{n,\gamma}^{\text{th}}$  stems from  $1^-$  resonances. Therefore, we performed calculations for a set

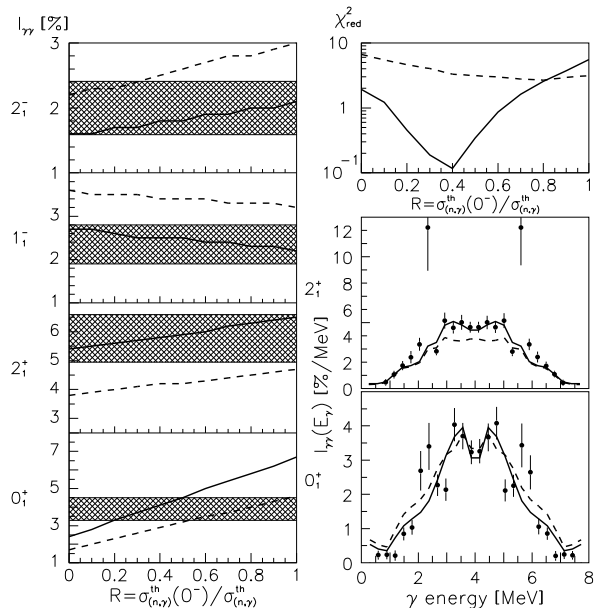


FIG. 3: Left: experimental values (hatched areas) for TSC intensities to final states (from top to bottom)  $2_1^-$  at 1198 keV,  $1_1^-$  at 1155 keV,  $2_1^+$  at 79 keV, and the  $0_1^+$  ground state compared to calculations as function of  $R$ . Included are statistical errors and systematical errors from normalization and detection efficiency, the latter two being correlated for all final levels. Solid and dashed lines correspond to  $M1$  and  $E1$  hypotheses for the soft resonance. Right: combined  $\chi_{\text{red}}^2$  for all four TSC intensities as function of  $R$  for the  $M1$  and  $E1$  hypotheses (upper panel). Experimental (filled circles) and calculated TSC spectra to the  $2_1^+$  state (middle panel) and  $0_1^+$  state (lower panel) for the  $M1$  hypothesis at  $R = 0.4$  and the  $E1$  hypothesis at  $R = 0.8$ . At  $\sim 2$  MeV, Porter-Thomas fluctuations in the experimental spectra become visible.

of ratios  $R = \sigma_{n,\gamma}^{\text{th}}(0^-) / \sigma_{n,\gamma}^{\text{th}}$ . These calculations show, however, that only the TSC intensity to the  $0_1^+$  state has a strong dependence on this ratio. Total experimental and calculated TSC intensities are shown in the left panels of Fig. 3. The calculations assuming  $E1$  for the soft resonance do not reproduce the experimental intensities consistently for any value of  $R$ . Good agreement is achieved assuming  $M1$  with the additional condition of  $R \sim 0.4$  for the  $0_1^+$  final state. However, it has to be emphasized that the conclusion of an  $M1$  multipolarity for the soft resonance can be established from the TSC intensities to the  $2_1^+$ ,  $1_1^-$ , and  $2_1^-$  states independently, irrespective of the value of  $R$ . Possible systematic uncertainties in the absolute normalization cannot change this conclusion, since in the case of the final state  $2_1^+$ , one would need a *decrease* while at the same time, for the  $1_1^-$  final state one would need an *increase* in the experimental TSC intensities in order to accommodate the  $E1$  hypothesis. The combined  $\chi_{\text{red}}^2$  for all four TSC intensities as function of  $R$  is also given. The  $M1$  hypothesis yields

the global minimum for  $R = 0.4 \pm 0.25$  with  $\chi_{\text{red}}^2 = 0.1$  whereas the minimal  $\chi_{\text{red}}^2$  for the  $E1$  hypothesis is  $\sim 2.7$  for  $R \sim 0.8$ . Finally, we show the TSC spectra to two final states compared to calculations using the  $M1$  hypothesis at  $R = 0.4$  and the  $E1$  hypothesis at  $R = 0.8$ . No further conclusions have been drawn from this comparison, however.

The integrated strength of the soft resonance is expressed as

$$B(M1 \uparrow) = \frac{9\hbar c}{32\pi^2} \left( \frac{\sigma\Gamma}{E} \right)_{\text{soft}} \quad (5)$$

giving a value of  $6.5(15) \mu_N^2$  which is entirely determined from the Oslo-type experiment after  $M1$  multipolarity has been established. This is in agreement with the sum-rule approach for soft, orbital  $M1$  strength [26] but is more than twice the strength reported from nuclear resonance fluorescence (NRF) experiments [27]. However, in [10, 28] several limitations in determining  $B(M1 \uparrow)$  using NRF are discussed, all resulting in possible underestimation. Concerns are that (i) too few  $1^+$  levels are observed in NRF experiments compared to level density estimates, (ii) the assumption in NRF experiments that the total radiative width equals the sum of the partial radiative widths for transitions to the ground state and the first excited state is not fulfilled, and (iii) the excitation-energy coverage is insufficient. Also in [10] a soft resonance with  $B(M1 \uparrow) \sim 7\mu_N^2$  is required in order to reproduce TSC spectra in  $^{163}\text{Dy}$ .

In conclusion, the soft resonance found in the RSF of  $^{172}\text{Yb}$  in Oslo-type experiments has been determined to be of  $M1$  multipolarity by an auxiliary TSC measurement. The strength of the  $M1$  resonance is  $B(M1 \uparrow) = 6.5(15) \mu_N^2$  which is entirely determined by the former experiment. This value agrees with a sum-rule approach for orbital strength, but is more than twice the value reported by NRF experiments. Assuming  $M1$  multipolarity for similar soft resonances in other rare earth nuclei gives consistent strengths of  $\sim 6 \mu_N^2$  for various even and odd Dy, Er, and Yb nuclei and reduced strengths of  $\sim 3 \mu_N^2$  for the more spherical Sm nuclei [29]. The centroids of the resonances increase weakly with mass number.

This work has benefited from the use of the Los Alamos Neutron Science Center at the Los Alamos National Laboratory. This facility is funded by the U.S. Department of Energy under Contract W-7405-ENG-36. Part of this work was performed under the auspices of the U.S. Department of Energy by the University of California, Lawrence Livermore National Laboratory under Contract W-7405-ENG-48, and Los Alamos National Laboratory under Contract W-7405-ENG-36. Financial support from the Norwegian Research Council (NFR) is gratefully acknowledged. A.V. acknowledges support from a NATO Science Fellowship under project number

150027/432. E.A. acknowledges support by U.S. Department of Energy Grant No. DE-FG02-97-ER41042. We thank Gail F. Eaton for making the targets.

---

\* Electronic address: schiller@nsl.msu.edu

- [1] G.A. Bartholomew *et al.*, Adv. Nucl. Phys. **7**, 229 (1973).
- [2] Samuel S. Dietrich and Barry B. Berman, At. Data Nucl. Data Tables **38**, 199 (1988).
- [3] J. Kopecky and M. Uhl, in Proceedings of a Specialists' Meeting on Measurement, Calculation and Evaluation of Photon Production Data, Bologna, Italy, 1994, Report No. NEA/NSC/DOC(95)1, p. 119.
- [4] A. Schiller *et al.*, Nucl. Instrum. Methods Phys. Res. A **447**, 498 (2000).
- [5] A. Voinov *et al.*, Phys. Rev. C **63**, 044313 (2001).
- [6] S.G. Kadmskiĭ, V.P. Markushev, and V.I. Furman, Yad. Fiz. **37**, 277 (1983) [Sov. J. Nucl. Phys. **37**, 165 (1983)].
- [7] *Handbook for Calculations of Nuclear Reaction Data* (IAEA, Vienna, 1998).
- [8] A. Voinov *et al.*, Nucl. Instrum. Methods Phys. Res. A **497**, 350 (2003).
- [9] A.M. Hoogenboom, Nucl. Instrum. Methods Phys. Res. **3**, 57 (1958); S.T. Boneva *et al.*, Fiz. Elem. Chastits At. Yadra **22**, 479, 1433 (1991) [Sov. J. Part. Nucl. **22**, 232, 698 (1991)].
- [10] F. Bečvář *et al.*, Phys. Rev. C **52**, 1278 (1995).
- [11] One assumes that only neutron  $s$  capture occurs.
- [12] C.E. Porter and R.G. Thomas, Phys. Rev. **104**, 483 (1956).
- [13] A. Gilbert and A.G.W. Cameron, Can. J. Phys. **43**, 1446 (1965).
- [14] M. Guttormsen *et al.*, Phys. Rev. C **68**, 064306 (2003).
- [15] M. Guttormsen *et al.*, Nucl. Instrum. Methods Phys. Res. A **374**, 371 (1996).
- [16] M. Guttormsen, T. Ramsøy, and J. Rekdal, Nucl. Instrum. Methods Phys. Res. A **255**, 518 (1987).
- [17] D.M. Brink, Ph.D. thesis, Oxford University, 1955; P. Axel, Phys. Rev. **126**, 671 (1962).
- [18] W.V. Prestwich, M.A. Islam, and T.J. Kennett, Z. Phys. A **315**, 103 (1984).
- [19] R. Firestone and V.S. Shirley, *Table of Isotopes*, 8th ed. (Wiley, New York, 1996).
- [20] R.C. Greenwood, C.W. Reich, and S.H. Vegors Jr., Nucl. Phys. **A252**, 260 (1975).
- [21] The cited parameters are mean values obtained from the  $^{173}\text{Yb}(^3\text{He},\alpha\gamma)^{172}\text{Yb}$  and  $^{172}\text{Yb}(^3\text{He},^3\text{He}'\gamma)^{172}\text{Yb}$  reaction data.
- [22] C. Coceva, A. Brusegan, and C. van der Vorst, Nucl. Instrum. Methods Phys. Res. A **378**, 511 (1996).
- [23] R. Firestone, private communication.
- [24] S.F. Mughabghab *Neutron Cross Sections*, (Academic Press, New York, 1984), Vol. I, part B.
- [25] W. Gelletly *et al.*, J. Phys. G **11**, 1055 (1985).
- [26] E. Lipparini and S. Stringari, Phys. Rep. **175**, 103 (1989).
- [27] A. Zilges *et al.*, Nucl. Phys. **A507**, 399 (1990); **A519**, 848 (1990).
- [28] A. Schiller *et al.*, preprint nucl-ex/0011018.
- [29] S. Siem *et al.*, Phys. Rev. C **65**, 044318 (2002).